Supplementary Information

Amplifying dual-visible-light photoswitching in aqueous media via confinement promoted triplet-triplet energy transfer

Wenhui Wang,[‡a] Weixin Yang,[‡a] Zhiwei Zhang,[‡a] Jinghong Dai,[a] Yisheng Xu,[b] Junji Zhang[a*]

[a]Key Laboratory for Advanced Materials and Joint International Research Laboratory of Precision Chemistry and Molecular Engineering, Feringa Nobel Prize Scientist Joint Research Center, School of Chemistry and Molecular Engineering, East China University of Science & Technology, 130 Meilong Road, Shanghai, 200237, China

[b]State Key Laboratory of Chemical Engineering, East China University of Science & Technology, 130 Meilong Road, Shanghai, 200237, China

‡These authors contributed equally: Wenhui Wang, Weixin Yang, Zhiwei Zhang

Email addresses: zhangjunji@ecust.edu.cn (J. Z.)

Table of Contents

1. Materials and Methods

1.1 General Methods

All starting reagents were commercially available and analytical purity without further treatment. **4CzIPN** were purchased from Xi'an Polymer Light Technology Corp. **mPEG-DSPE** were purchased from Laysan Bio, Inc. TLC analysis was performed on silica-gel plates and column chromatography was conducted using silica-gel column packages purchased from Yantai HuangHai Chemical (China). NMR spectra were recorded on Bruker AM-400 spectrometers with tetramethylsilane (TMS) as an internal reference, $CDCl_3$ as the solvent. UV/Vis spectra were recorded on Varian Cary 500 (1 cm quartz cell). Emission spectra and fluorescence lifetime were acquired on Edinburgh Instruments Fluorescence Spectrometer FLS1000 fluorimeter.The photochromic reaction as well as quantum yields was carried by irradiation using a adjustable-power LED lamp (PerfectLight, PLS-LED1000C, 100 W) equipped with different wavelengths light box.

Nanosecond Transient absorption measurements were performed on LP-980 laser flash photolysis spectrometer setup (Edinburgh Instruments, UK). Excitation was performed using the third harmonic (355 nm, 100 mJ, 10 ns, 10 Hz) of a Q–switched Nd:YAG laser. The probe light was provided by a 450 W Xe arc lamp. These two light beams were focused onto a 1 cm quartz cell. The signals analyzed by a symmetrical Czerny-Turner monochromator were detected by a Hamamatsu R928 photomultiplier, and the signal was processed via an interfaced computer and analytical software. All samples were prepared with three freeze–pump–thaw cycles and kept under an argon atmosphere. All tests were carried on at room temperature.

1.2 Preparation of Phosphate Buffered Saline

NaCl (8 g), KCl (0.2 g), Na_2HPO_4 (1.44 g), KH_2PO_4 (0.24 g) were dissolved in 800 mL distilled water and the solution was adjusted pH to 7.4 with HCl. Then add water to 1000 mL. After high pressure steam sterilization, store at room temperature.

1.3 Preparation of Micelle

The typical procedure for particle preparation using the CIJ-D mixer was shown in **Figure S1**. For the organic phase, **DAE** (0.828 mg) and **4CzIPN** (1.576 mg) were dissolved in 2 mL THF. The amphiphilic polymer **mPEG-DSPE** (24.04 mg) were dissolved in phosphate Buffered Saline (PBS) with pH of 7.4 (2 mL) acted as the aqueous. The exit stream outlet was submerged in 16 mL PBS. The two syringes were then pushed rapidly to inject the liquids into the CIJ-D mixer at the equal flow rates, where the two streams were vigorously mixed. The final micelle suspension was dialyzed against PBS (pH =7.4) for 24 h to remove THF completely. The micelle was stored at room temperature and can remain stable for more than 28 days.

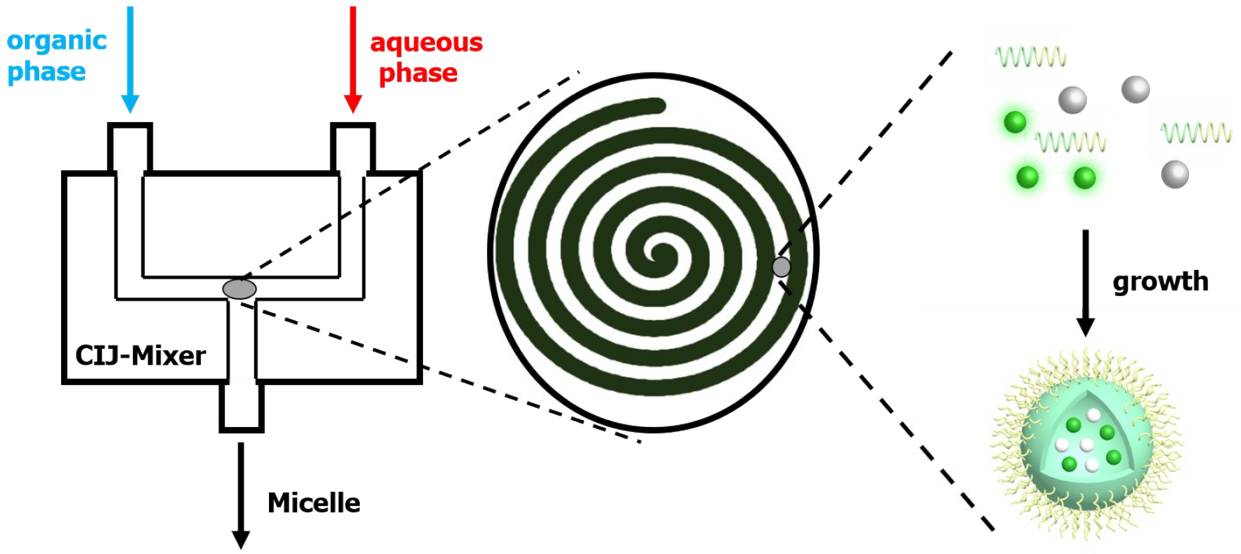

Figure S1. The CIJ-D mixer and micelle preparation process.

1.4 Synthesis of DAE

Compound 1 were prepared according to literatures reported previously[1]. Detailed synthetic procedures are described below.

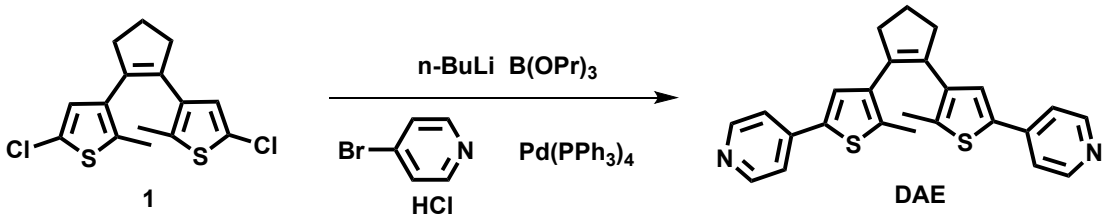

1,2-Bis-(2-chloro-5-methylthien-4-yl)-cyclopentene (compound **1**) (1.0 g, 3.06 mmol) was dissolved in 10 mL of dry THF and cooled to -78 °C under argon. To this solution *n*-BuLi (2.2 M in hexane, 3.1 mL, 6.82 mmol) was slowly added and the mixture was stirred for 1 h at this temperature. Then $B(OPr)_3$ (1.77 mL, 7.65 mmol) was dropped into the solution and stirred for 1 h at room temperature. 4-bromopyridine hydrochloride (1.18 g, 6.12 mmol) was dissolved in 5 mL of degassed THF under argon. $Pd(PPh_3)_4$ (100 mg, 0.086 mmol) was added to the second solution followed by addition of 10 mL of degassed aqueous of 2.5 M sodium carbonate solution. The first solution was added to the second without further purification and the mixture was refluxed for 16 h. The aqueous phase was extracted with DCM and the organic phase was washed with saturated NaCl aqueous, then dried over $MgSO_4$ and evaporated in reduced pressure. The crude product was purified by column chromatography on silica gel (EA : DCM = 1 : 1) to obtain DAE after drying in vacuo as colorless solid (0.72 g, 56.9%). H NMR (400 MHz, $CDCl_3$) δ 8.53 (d, J = 5.9 Hz, 4H), 7.38 – 7.32 (m, 4H), 7.22 (s, 2H), 2.86 (t, J = 7.4 Hz, 4H), 2.12 (dt, J = 14.8, 7.5 Hz, 2H), 2.02 (s, 6H).

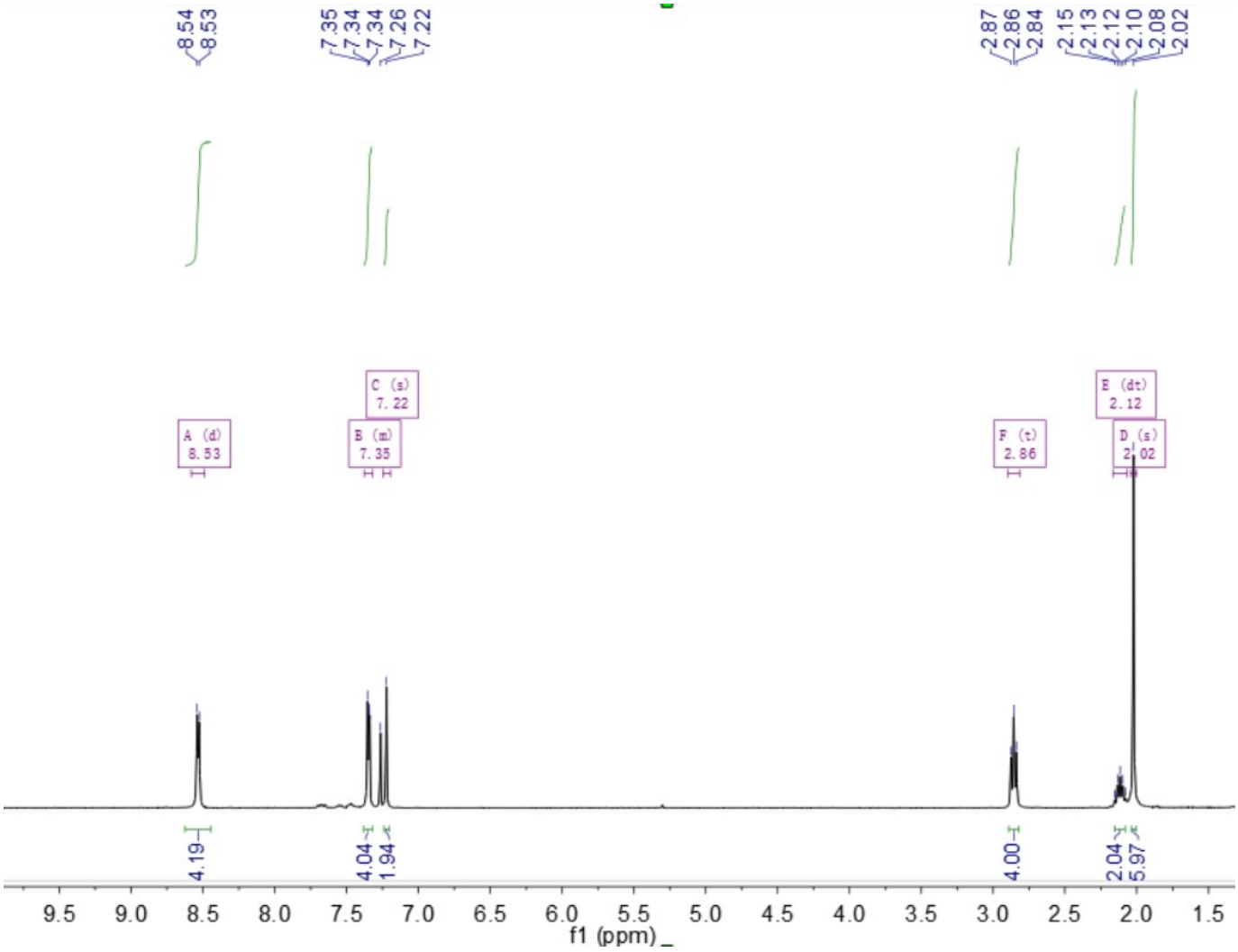

Figure S2. ^{1}H NMR spectrum of **DAE**.

1.5 Confocal and FLIM Imaging

Cells cultured in growth medium supplemented with 10% FBS were added to a glass-bottom confocal dish. Cells were maintained in a humidified atmosphere of 5% CO_2 and 95% air at 37 °C overnight. Then, cells were incubated sequentially with **DS@M** for 30 min. Then the cells on the microplate were rinsed by warm PBS and fixed by 4% paraformaldehyde for 20 min at room temperature. Immediately after sealing, the fluorescence intensity and lifetime was detected and photographed with confocal laser scanning microscopy and fluorescence lifetime imaging microscopy, respectively (Leica TCS SP8, Leica Microsystems, Wetzlar, Germany, green channel excitation: 475 nm, emission: 500-650 nm).

1.6 Micelle/Organelles Colocalization

Lysosomes, and mitochondria were selected as the test organelles. The cell culture procedure was same as confocal iamging.Firstly, the cells were incubated sequentially with **DS@M** (10 μM) for 30 min. Then, Lyso-Tracker Red and Mito-Tracker Deep Red 633 were added and incubated for 30 min, respectively. Then the cells on the microplate were rinsed by warm PBS. The colocalization between **DS@M** and lysosomes or mitochondria was observed using CLSM. Quantification of the colocalization efficiency was conducted using Pearson's correlation and the CLSM software. The value of Pearson's correlation is range from -1.0 to 1.0. In general, when the correlation is higher than 0.5, it can be considered the existence of colocalization phenomenon. The closer to 1 indicates the more significant colocalization.

1.7 STORM Imaging Protocol

Super-resolution STORM imaging was performed on a Nikon N-STORM microscope53 equipped with a motorized inverted microscope ECLIPSE Ti-E, an Apochromat TIRF 100 × oil immersion lens with a numerical aperture of 1.49 (Nikon), an electron multiplying charge-coupled device (EMCCD) camera (iXon3 DU-897E, Andor Technology), a quad band filter composed of a quad line beam splitter (zt 405/488/561/640rpc TIRF, Chroma Technology Corporation) and a quad line emission filter (brightline HC 446, 523, 600, 677, Semrock, Inc.). The TIRF angle was adjusted to oblique incidence excitation at the value of 3920-3950, allowing the capture of images at about 1 μm depth of samples. The focus was

kept stable during acquisition using Nikon focus system. Before the STORM imaging experiments, we first confirmed the feasibility of micelle imaging using total internal reflection (TIRF) excitation at 488 nm and detection with a 560/60 nm bandpass filter. Furthermore, the fluorescence quenching amplification was proved to be efficient under 488 nm laser irradiation by modulate the photochromic processes. During the imaging experiments, the dark state (**DAE-c** + **4CzIPN**) was converted to the fluorescent state (**DAE-o** + **4CzIPN**) under 561 nm visible light. Then, the 488 nm laser was used for switching back the fluorophores from dark to the fluorescent state, meanwhile the 488 nm laser was used to excite the 4CzIPN for collecting the cell images. The integration time of the camera was 20 ms per frame. To achieve super-resolution imaging, cells were seeded on a glass dish, and when the density was appropriate, cells were stained with micelle (10 μM) for 30 min and cells were fixed with 4% paraformaldehyde, followed by three washes with PBS buffer.

2. The particle size characterization of DS@M

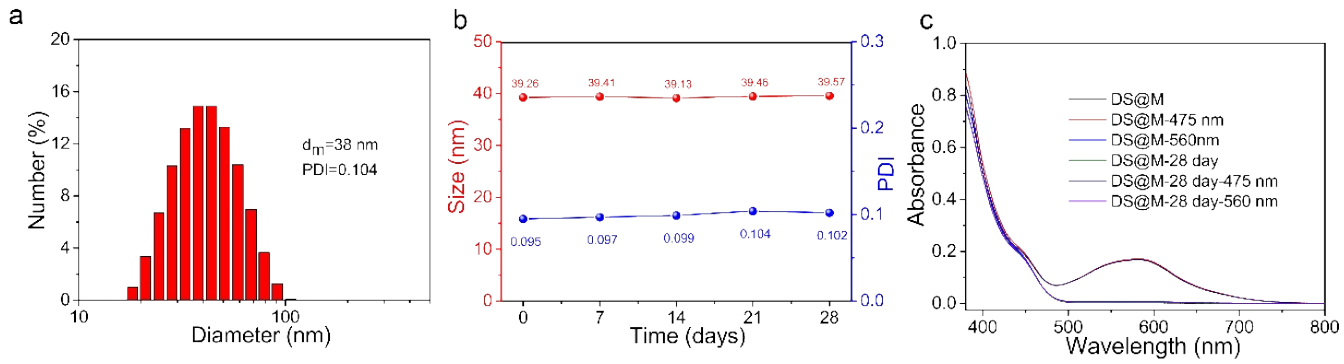

Figure S3. a) DLS histograms of **DS@M**; b) Changes of **DS@M** particle size (red circle) and PDI (blue circle) after stored at room temperature for 28 days in the dark; c) Photochromism of **DS@M** before and after stored at room temperature for 28 days in the dark.

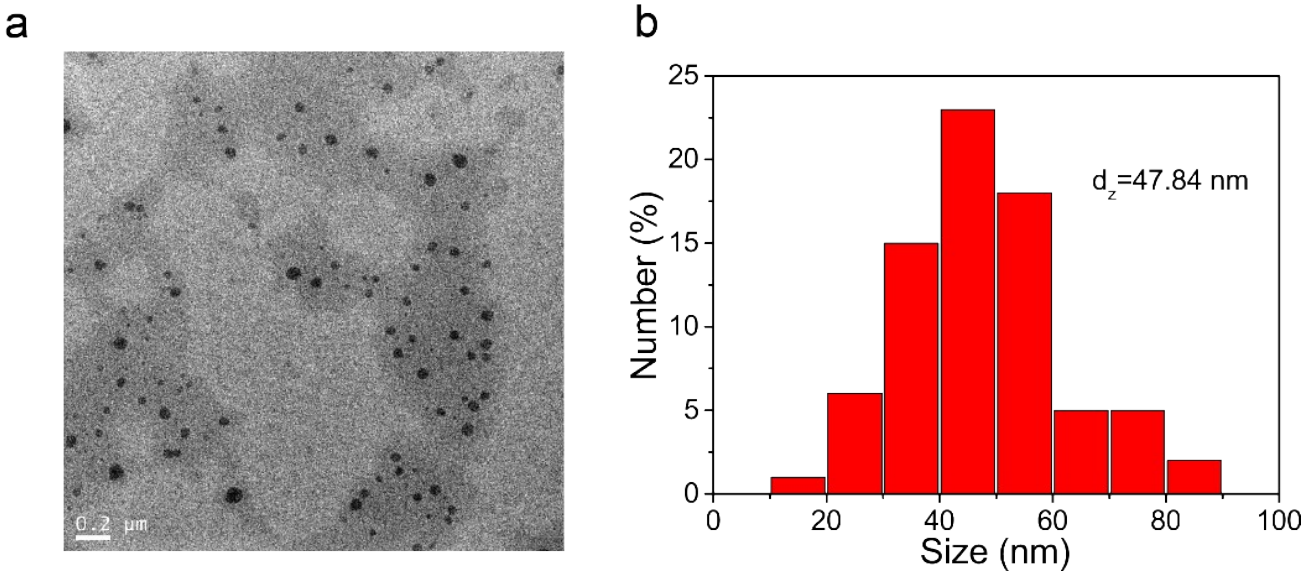

Figure S4. a) TEM image of **DS@M**, scale bar = 0.2 μm; b) Particle size statistical analysis of TEM image.

3. Absorption of DAE/4CzIPN and DS@M

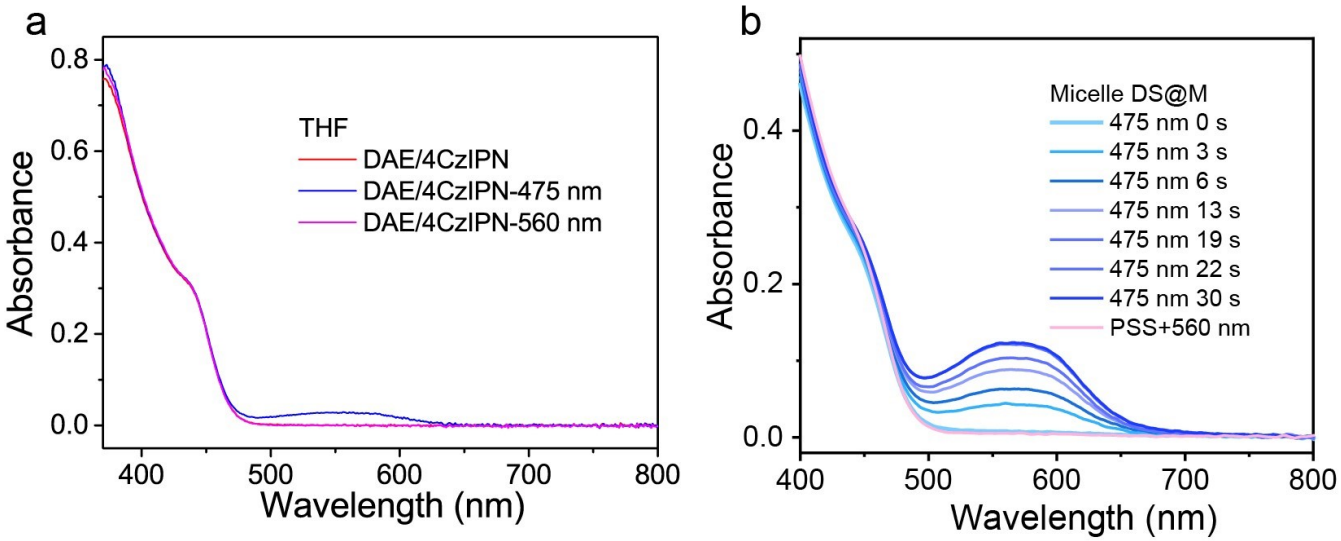

Figure S5. a) Absorption spectra of **DAE/4CzIPN** upon irradiation at 475 nm and 560 nm, performed in 2 mL THF, 2.5×10^{-5} M. b) Absorption spectra of **DS@M** gradually reaching photo-stationary state (PSS) upon irradiation at 475 nm, and returning to the original open state via 560 nm irradiation, performed in 2 mL PBS buffer, 2.5×10^{-5} M.

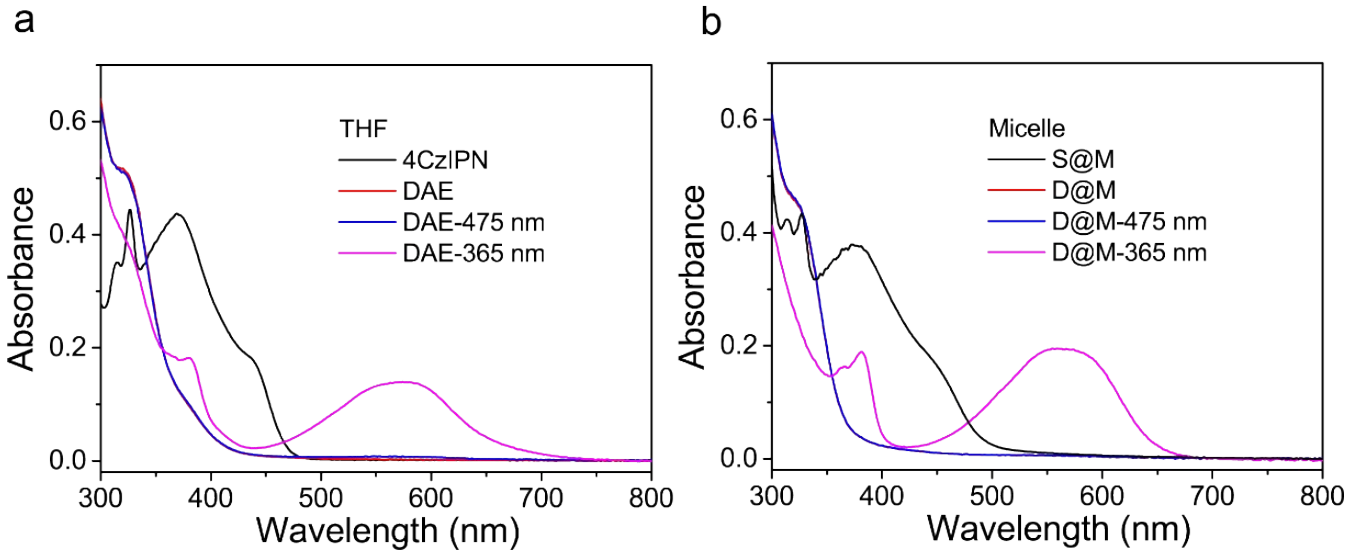

Figure S6. a) Absorption spectra of **DAE-o** (red), **4CzIPN** (black) and **DAE** upon irradiation with 365 nm (magenta) and 475 nm (blue), performed in 2 mL THF, 2.5×10^{-5} M. b) Absorption spectra of **D@M** (red), **S@M** (black) and **D@M** upon irradiation at 365 nm (magenta) and 475 nm (blue), performed in 2 mL PBS buffer, 2.5×10^{-5} M.

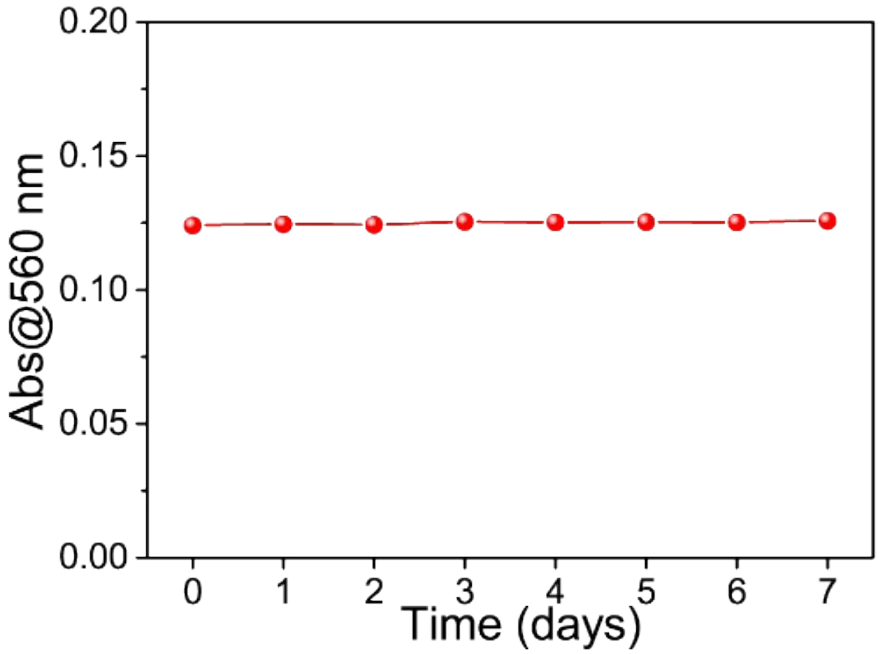

Figure S7. The thermo-stability of **DS@M** under room temperature in the dark.

4. Photochromic reaction quantum yields

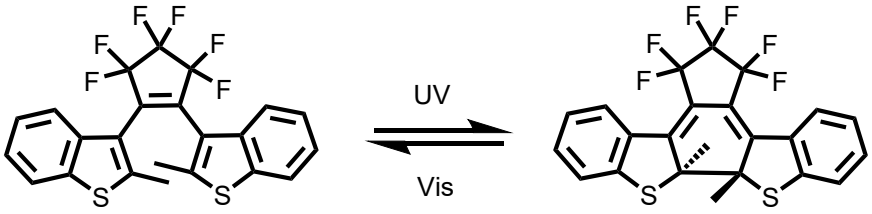

DAE-a-o **DAE-a-c**

The photoreaction quantum yields of **DAE/4CzIPN** at 313 nm, 475 nm and 560 nm in different system were measured with **DAE-a** as the actinometer.[2] The quantum yields of **DAE-a** at different wavelengths is respectively 0.31(313 nm), 0.3048(475 nm), 0.2763(560 nm). The extinction coefficient of **DAE-a** at different wavelengths is respectively 4715 M^{-1} cm^{-1} (313 nm), 6480 M^{-1} cm^{-1} (475 nm), 4585 M^{-1} cm^{-1} (560 nm). Under the same conditions, the number of photons arriving in the cuvette per unit time can be obtained by the actinometer.

The photochromic reaction quantum yield (Φ_x) of the diarylethene derivative is defined as Eq. 1,

$$\Phi_x = \frac{-\frac{dn_m}{dt}}{n_p(1-10^{-A'})} \quad \text{Eq. 1}$$

where n_m is the number of molecules that undergo photochromic reaction, n_p is irradiation photon number per second at irradiation wavelength, A is the absorbance of the closed-ring isomer at irradiation wavelength. Based on Lambert-Beer's law, A is expressed as Eq. 2,

$$A = \varepsilon \times \frac{n_m}{N_A} \times \frac{1000}{v} \times l \quad \text{Eq. 2}$$

where ε is the absorption coefficient of the closed-ring isomer (M^{-1} cm^{-1}), N_A is Avogadro's number, v is solution volume (cm^3), l is cell length (cm). From Eq. 1 and 2, Φ_x is expressed as follows:

$$\Phi_x = \frac{-N_A v\frac{dA}{dt}}{1000\varepsilon l n_p(1-10^{-A'})} \quad \text{Eq. 3}$$

When $A=A'$:

$$\int_{A(0)}^{A(t)} \frac{10^A}{10^A-1}dA = -\frac{1000\varepsilon l n_p \Phi_x}{N_A v}\int_0^t dt \quad \text{Eq. 4}$$

$$\log\left(10^{A(t)}-1\right) - \log\left(10^{A(0)}-1\right) = -\frac{1000\varepsilon l n_p \Phi_x}{N_A v}t \quad \text{Eq. 5}$$

When $A\neq A'$ and A' is not changing in time:

$$A(t) - A(0) = -\frac{1000\varepsilon l n_p (1 - 10^{-A'})\Phi_x}{N_A v} t \quad \text{Eq. 6}$$

where, *A(t)* is the change of absorbance upon irradiation at detection wavelength, *A'* is the absorbance upon irradiation at excitation wavelength, ε is the extinction coefficient at detection wavelength ($\varepsilon_{560\,nm}$ = 23688 M^{-1} cm^{-1}) and n_p is irradiation photon number per second at irradiation wavelength, calculated by the actinometer **DAE-a**. When calculating the photoreaction quantum yields at 475 nm and 313 nm, Eq. 6 is used. When calculating the photoreaction quantum yields at 560 nm, Eq. 5 is used.

5. The confirmation of triplet-triplet energy transfer

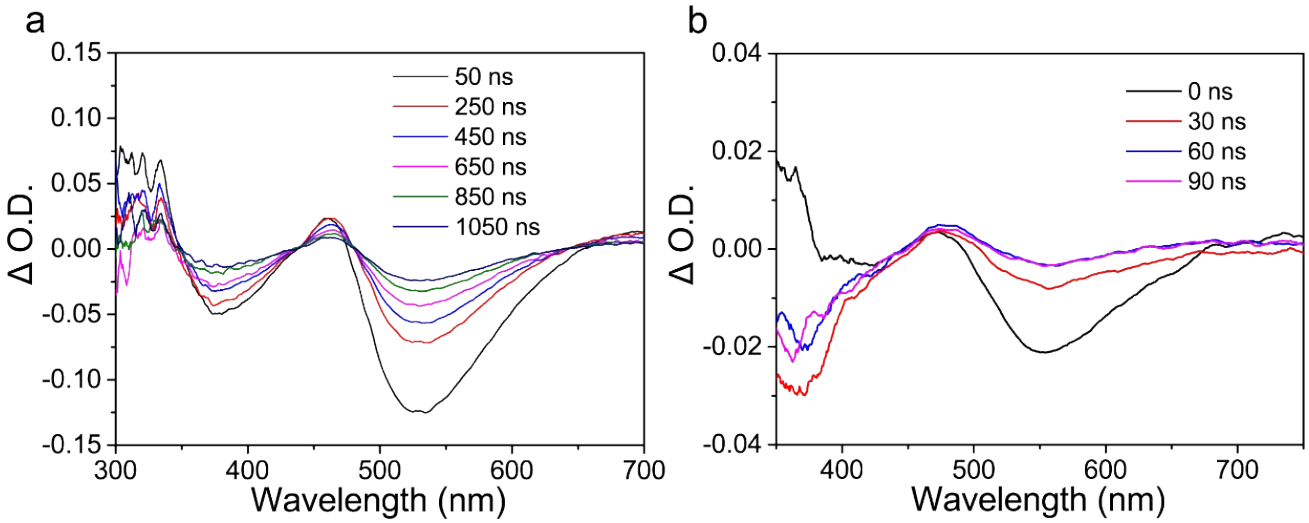

Figure S8. a) Nanosecond time-resolved transient absorption spectra of **DAE/4CzIPN** in 3 mL THF, 1×10^{-4} M; b) Nanosecond time-resolved transient absorption spectra of of **DS@M** in 3 mL PBS buffer, 1×10^{-4} M.

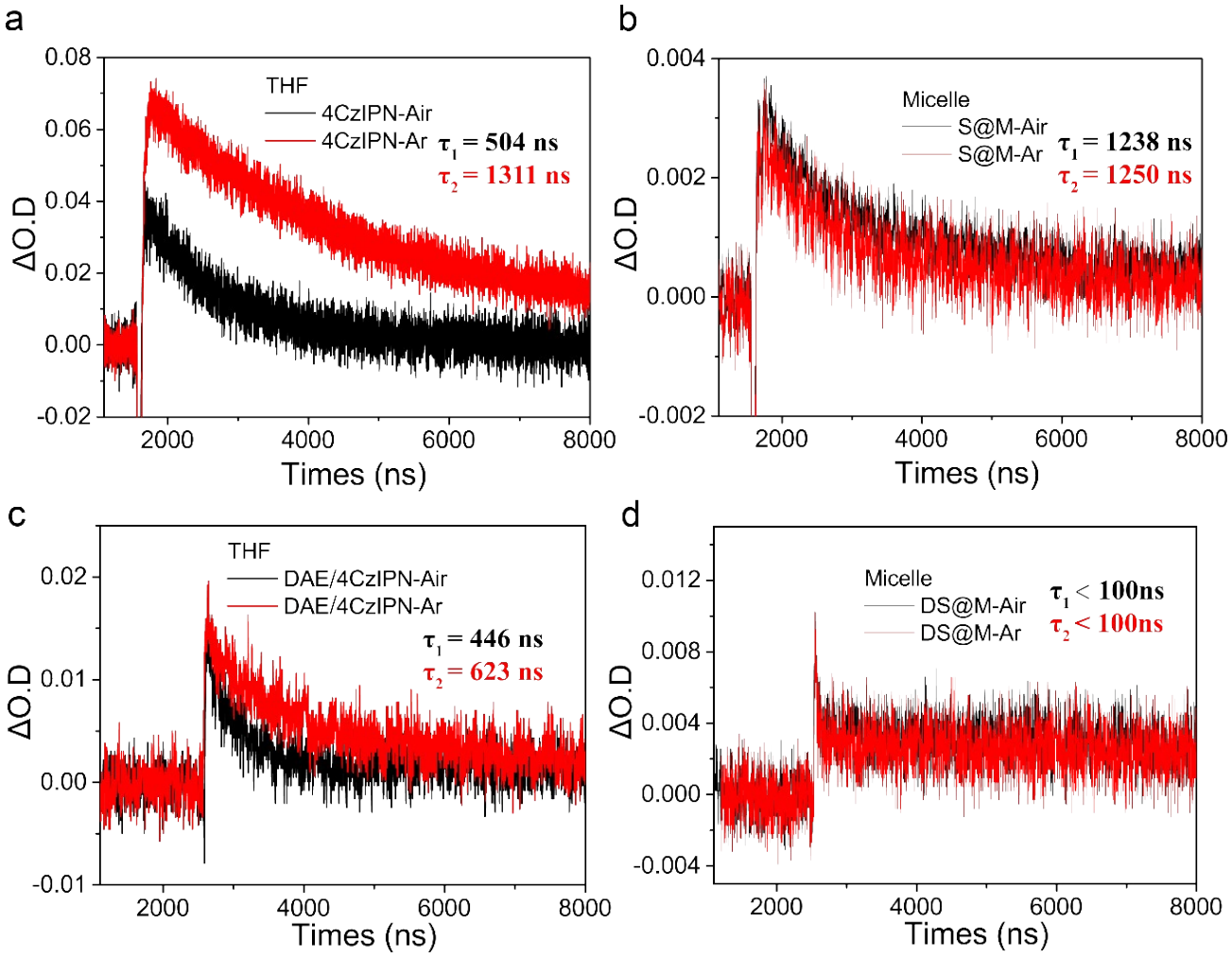

Figure S9. a) Transient absorption decays of **4CzIPN** (1×10^{-4} M in 3 mL THF) at 477 nm; b) Transient absorption decays of **S@M** (1×10^{-4} M in 3 mL PBS buffer) at 477 nm; c) Transient absorption decays of **DAE/4CzIPN** (1×10^{-4} M in 3 mL THF) at 477 nm; d) Transient absorption decays of **DS@M** (1×10^{-4} M in 3 mL PBS buffer) at 477 nm; black line is aerated and red line is deaerated.

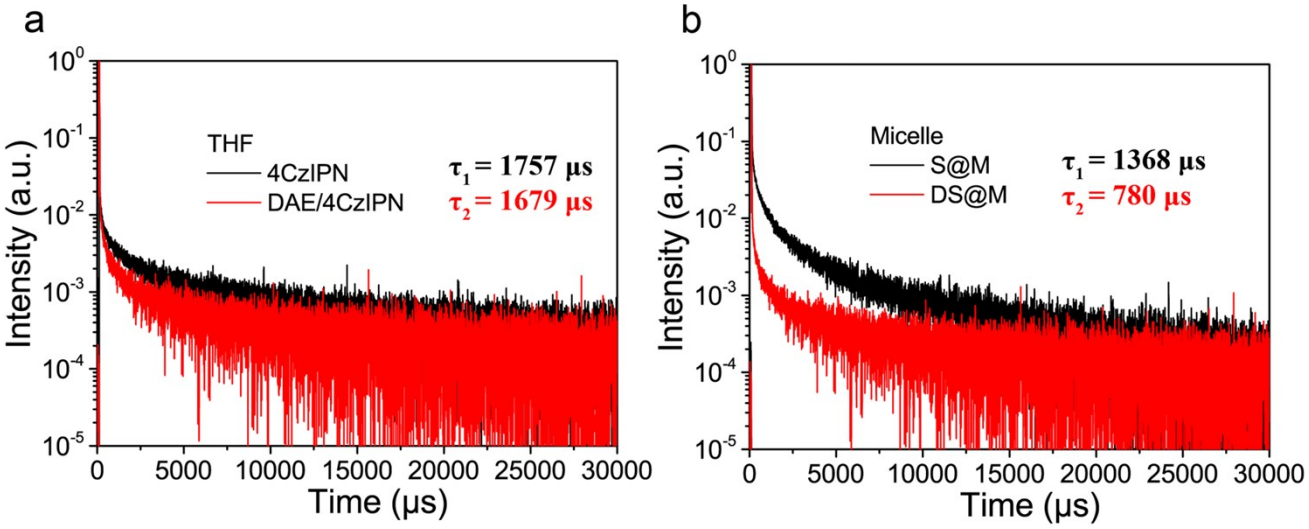

Figure S10. a) The emission decays of **4CzIPN** and **DAE/4CzIPN** at 77 K; b) The emission decays of **S@M** and **DS@M** at 77 K.

6. The oxygen-shielding effect of micelle nanoconfinement.

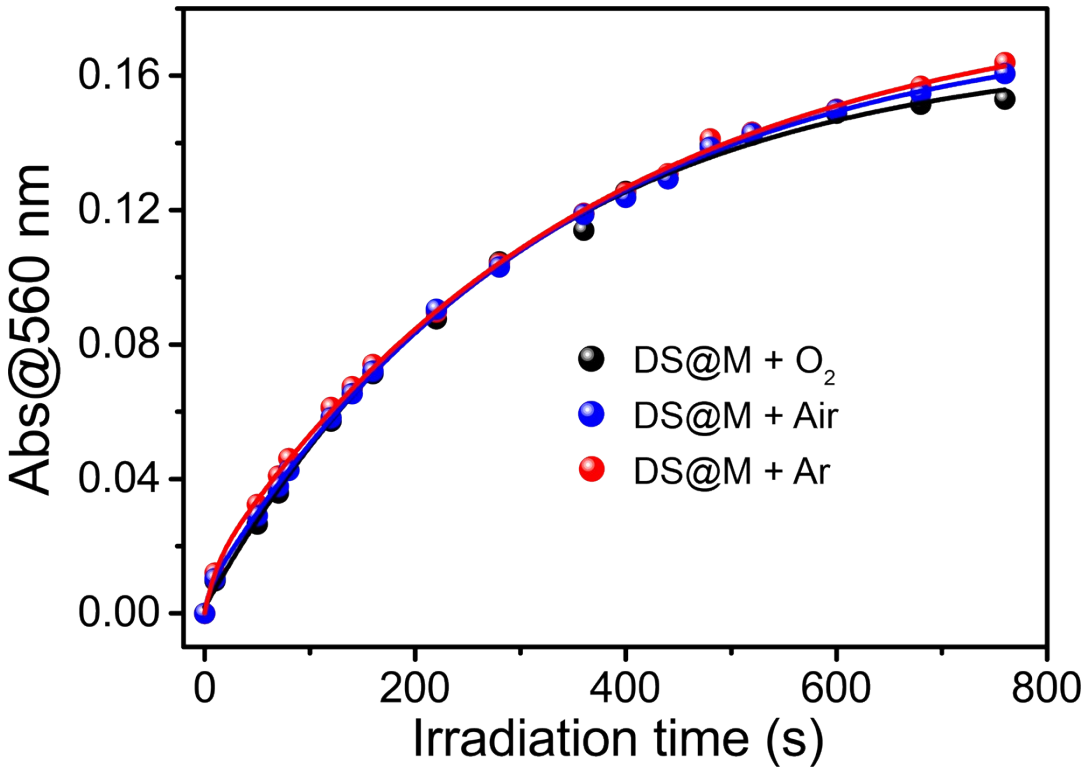

Figure S11. Photocyclization performances of **DS@M** (2.5×10^{-5} M in 2 mL PBS buffer) in de-aerated (argon bubbled) PBS buffer (red), PBS buffer with air bubbling (blue), PBS buffer with oxygen bubbling (black).

Table S1 Photochromic quantum yields of **DS@M** in different oxygen content system.

Photoreaction	**λ (nm)**	**Φ (%)**
DAE-o→DAE-c (with **4CzIPN** in **DS@M**)	475	7.75
DAE-o→DAE-c (with **4CzIPN** in **DS@M**, oxygen bubbling)	475	7.61
DAE-o→DAE-c (with **4CzIPN** in **DS@M**, argon bubbling)	475	8.61

Singlet oxygen quantum yield calculation

The general ROS generation measurements were conducted using 9,10-Anthracenediyl-bis(methylene)dimalonic acid (ADBA) as the indicator. The absorbance of each sample (1 μM) was firstly set as blank. Then, 10 μM of ABDA was mixed to each sample (DMSO/water (v:v) = 1/100) in dark room, and the absorbance of sample was measured at once. The sample mixture was then irradiated under white light (10 mW/cm^{-2}) at intervals of 20 s until 200 s. The absorption of ABDA at 378 nm was recorded at various irradiation times to obtain the decay rate of photosensi tizing process. The absorbance change of the same concentration ABDA alone in 200 s light irradiation time was deducted as blank.

Rose Bengal (RB) was employed as the standard photosensitizer. To eliminate the inner-filter effect, the absorption maxima were adjusted to ~0.2 OD. The measurements were carried out under white light irradiation in DMSO/water (v:v) = 1/100. Singlet oxygen quantum yields of the 4CzIPN (in bulk solution)/S@M/DS@M were calculated by the equation:

$$\Phi_O = \Phi_{RB}\frac{K_S}{K_{RB}}/\frac{A_{RB}}{A_S} \quad \text{Eq.7}$$

where K_S and K_{RB} represent the decomposition rate constants of ABDA with **4CzIPN** (in bulk solution)/**S@M**/**DS@M** and RB, respectively. A_S and A_{RB} represent the light absorbed by **4CzIPN** (in bulk solution)/**S@M**/**DS@M** and RB, respectively, which are determined by integration of the areas under the absorption bands in the wavelength range of 400-800 nm. Φ_O is the $^1O_2$ quantum yield of RB, which is 0.75 in water.

By Eq.7, the singlet oxygen quantum yield is calculated as:

Standard	Φ_O (%) **4CzIPN**	Φ_O (%) **S@M**	Φ_O (%) **DS@M**
RB	15.61	3.85	0.34

7. Solvent-dependent photochromic performance of DAE/4CzIPN

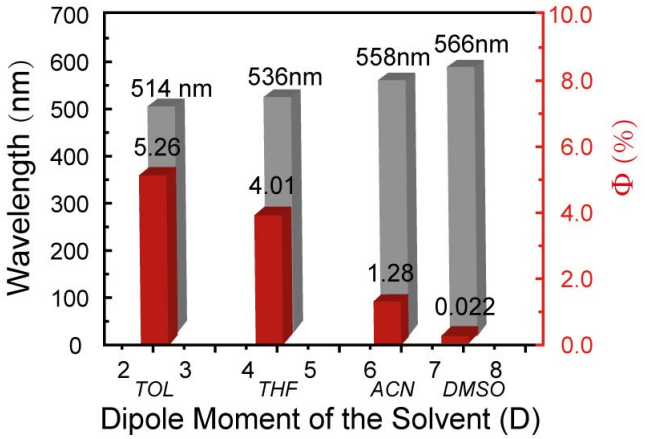

Figure S12. Solvent-dependent photochromic performance of **DAE/4CzIPN** (red column) and the emission wavelength of **DAE/4CzIPN** in different de-aerated solvents (TOL: toluene; THF: tetrahydrofuran; ACN: acetonitrile; DMSO: dimethylsulfoxide)(λ_{ex} = 365 nm, gray column), 2.5×10^{-5} M, 2 mL.

8. Density functional theory (DFT) calculation details

Table S2. The value of triplet (T_1) excited state energy for investigated compounds.

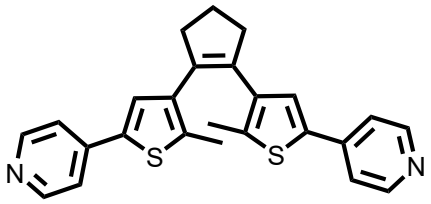 **DAE-o**	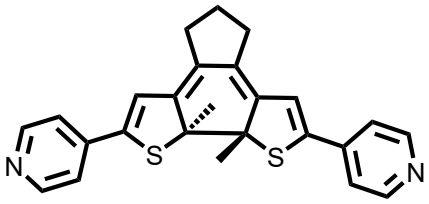 **DAE-c**	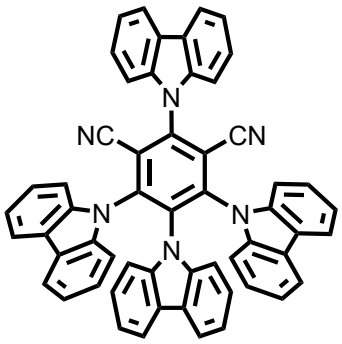 **4CzIPN**
Calculated: S_1 = 4.1932 eV T_1 = 2.4017 eV	Calculated: S_1 = 2.0224 eV T_1 = 0.4504 eV	Calculated: S_1 = 2.5572 eV T_1 = 2.4393 eV

Density functional theory (DFT) calculations were employed to optimize the ground state geometries of the molecules, using the B3LYP functional[3] and the 6-31G(d) basis set[4]. At the optimized geometries, time-dependent DFT (TDDFT) calculations were carried out using the PBE38 functional and the 6-311+G(d, p) basis set[5]. All calculations were carried out using the Gaussian09 program package[6].

Table S3. DFT calculations of energy values of investigated compounds.

Compound	Orbital	Energy (hartree)	Energy (eV)
DAE-o	HOMO-1	-0.23405	-6.36882
	HOMO	-0.21796	-5.93099
	LUMO	-0.06416	-1.74588
	LUMO+1	-0.06164	-1.67731
DAE-c	HOMO-1	-0.23038	-6.26896
	HOMO	-0.18673	-5.08118
	LUMO	-0.09848	-2.67978
	LUMO+1	-0.05947	-1.62561
4CzIPN	HOMO-1	-0.22290	-6.06542
	HOMO	-0.21729	-5.91277
	LUMO	-0.10236	-2.78536
	LUMO+1	-0.08918	-2.42671

9. Emission spectra and lifetime of DAE/4CzIPN and DS@M

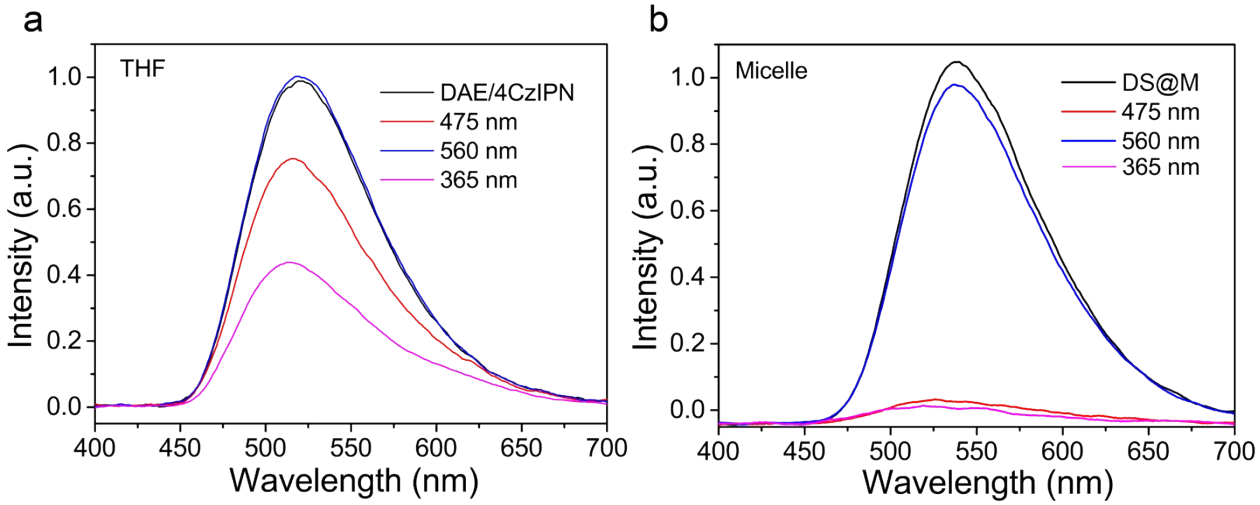

Figure S13. a) Emission spectra of **DAE/4CzIPN** (2.5×10^{-5} M) in 2 mL THF after irradiation at 475 nm, 365 nm and 560 nm, λ_{ex} = 365 nm; b) Emission spectra of **DS@M** (2.5×10^{-5} M) after irradiation at 475 nm and 560 nm in 2 mL PBS buffer, λ_{ex} = 365 nm.

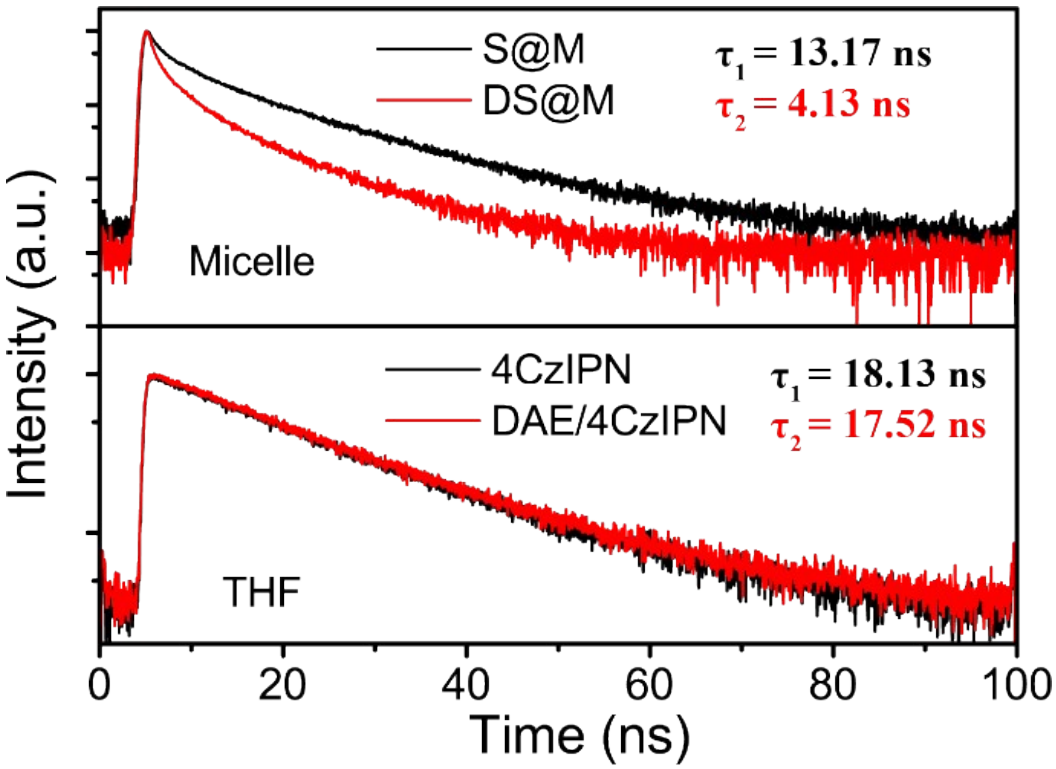

Figure S14. Top: Fluorescence emission decays of **S@M** and **DS@M** (in PSS) in 2 mL PBS buffer, 2.5 × 10^{-5} M; Bottom: Fluorescence emission decays of **4CzIPN** and **DAE/4CzIPN** (in PSS) in 2 mL THF, 2.5 × 10^{-5} M.

10. The Stern-Volmer plot of DAE/4CzIPN and DS@M

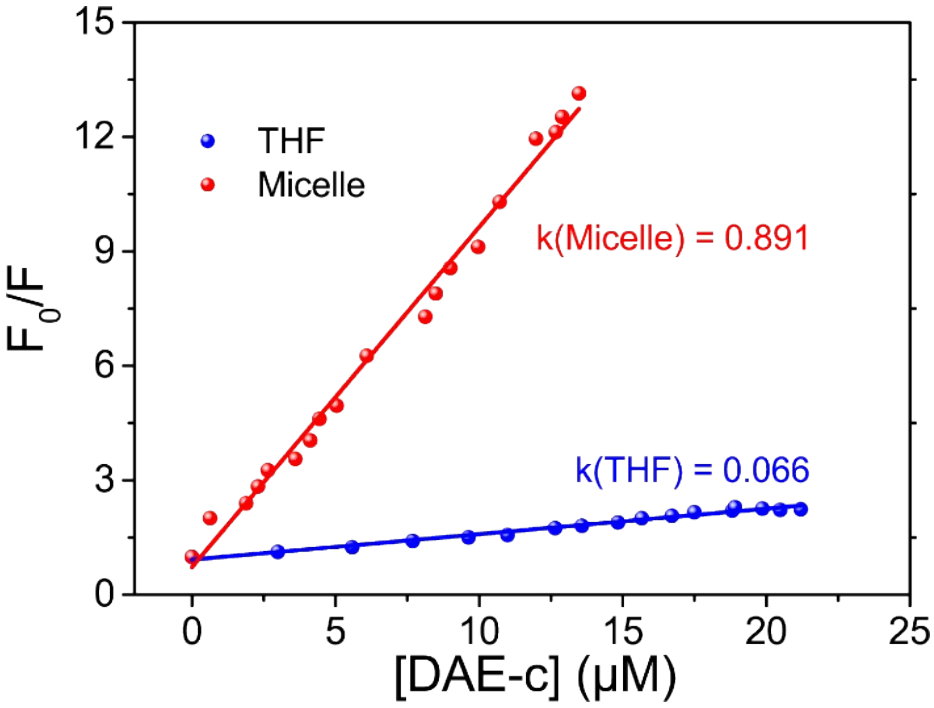

Figure S15. Stern-Volmer plot and linear fit for quenching of **DAE/4CzIPN** (blue line) and **DS@M** (red line).

11. The fatigue resistance of DS@M

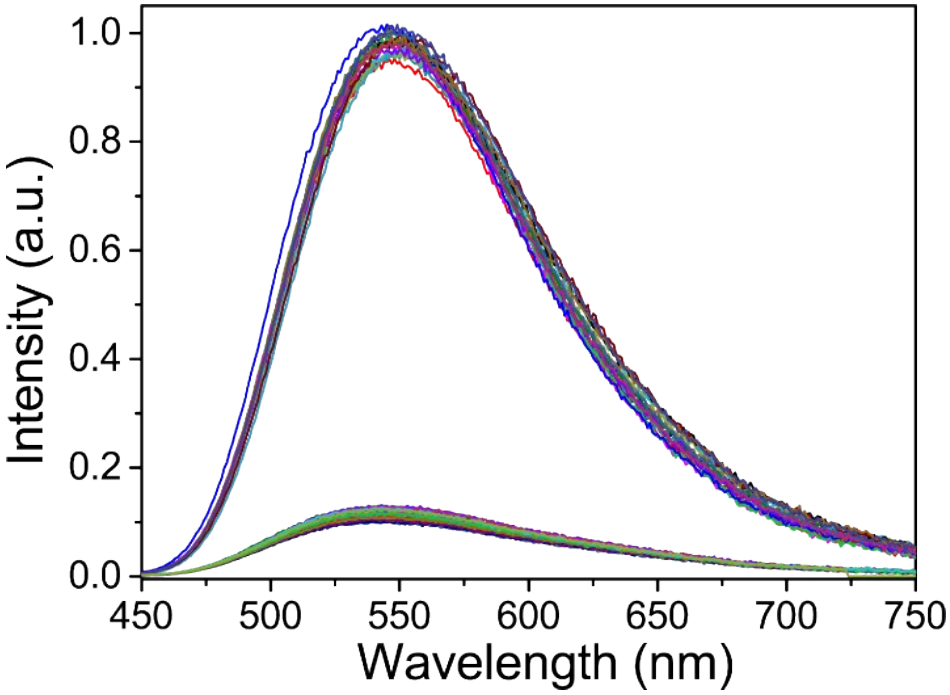

Figure S16. Emission spectra of **DS@M** (2.5×10^{-5} M) and upon irradiation at 475 nm and 560 nm for 20 cycles in 2 mL PBS buffer.

12. All-visible-light instant patterning application

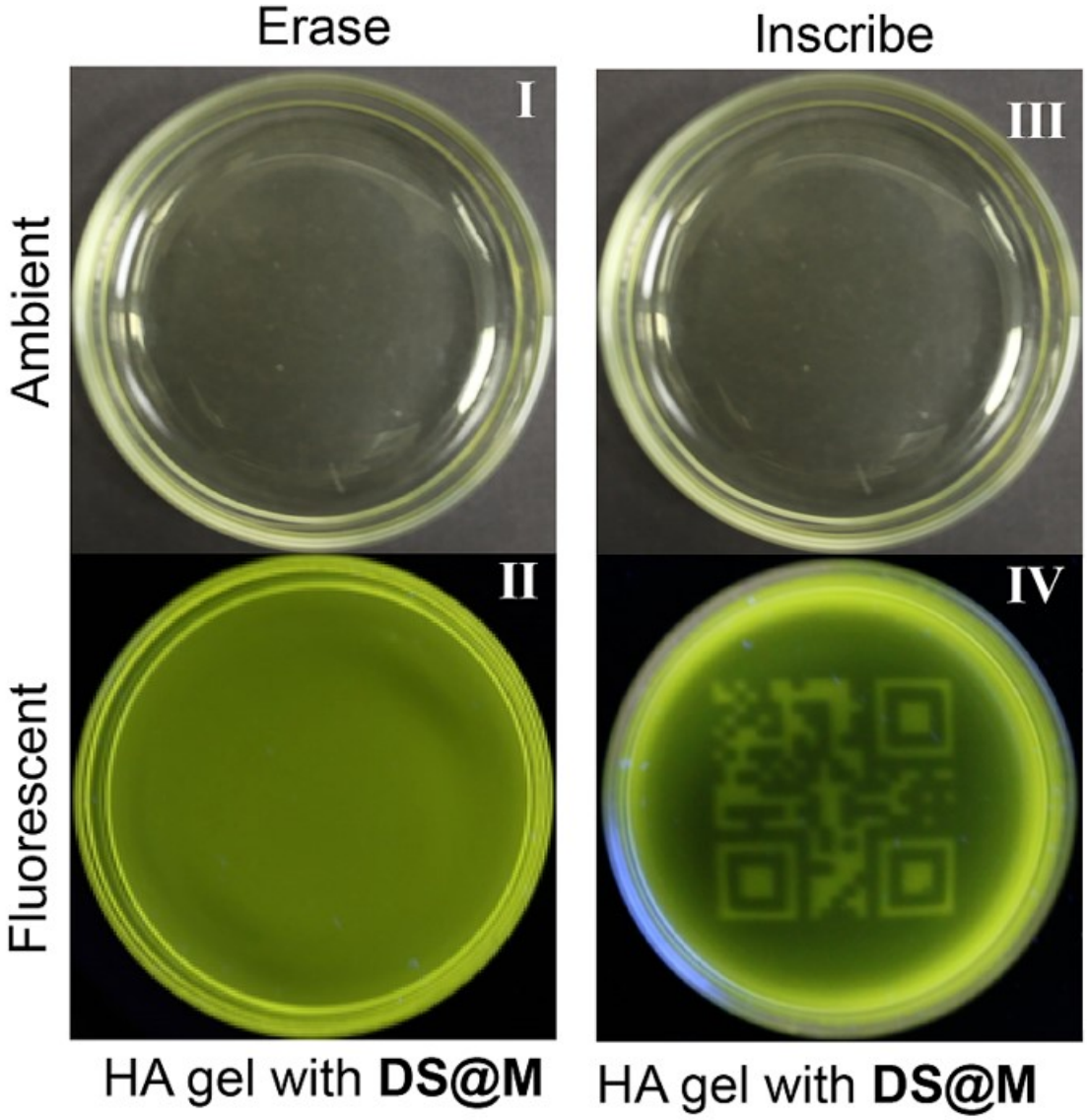

Figure S17. All-visible-light instant patterning application of **DS@M** in a hydrogel matrix. The fluorescent readable QR-code was inscribed onto and erased from **DS@M** dispersed hydrogel using 475 nm (10 mW/cm^2) and 560 nm (30 mW/cm^2) light.

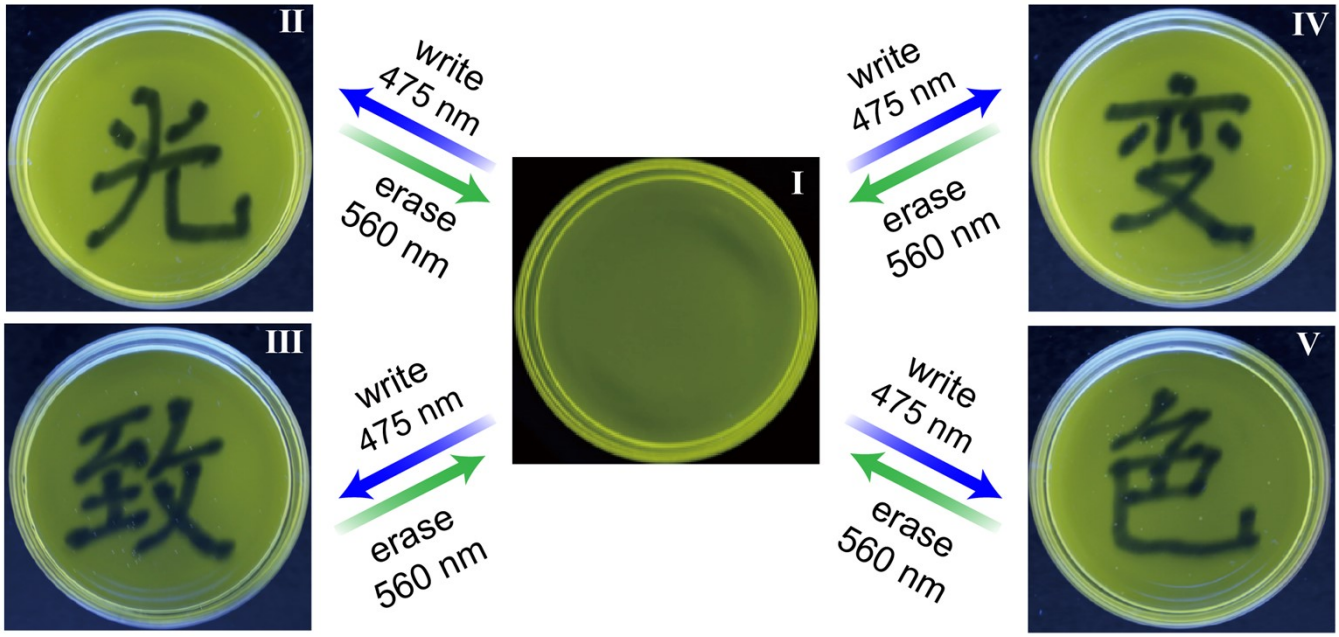

Figure S18. Four Chinese characters (together meaning "photochromism") were sequentially written onto and erased from the same hydrogel using hand-held 450 nm laser pointer and 560 nm irradiation, respectively.

13. Fluorescence Quantum Yields

The quantum yield of a fluorophore is by comparison with standards of known quantum yield. The quantum yield is determined by comparison of the wavelength integrated intensity of the emission spectrum of the fluorophore under examination to that of a suitable standard. The emission wavelength range and the shape of the spectra under comparison should match as much as possible, and the absorbance values should be kept below 0.1 to avoid inner filter effects. In these conditions, using the same excitation wavelength, the unknown quantum yield is calculated using:

$$\Phi_{PL} = \Phi_r \frac{I A_r n^2}{I_r A n_r^2} \quad \text{Eq. 8}$$

where Φ_{PL} is the quantum yield, I is the integrated emission intensity, A is the absorbanceat the excitation wavelength, and n is the refractive index of the solvent. The subscript r refers to the reference fluorophore of known quantum yield.

In order to reduce the error caused by non-overlapping emission wavelengths, we selected three standards to determine the fluorescence quantum yields.

Emission range (nm)	Compoound	Solvent	Φ_r (%)
400-600	B-Carboline	H_2SO_4 0.5 M	60
430-560	Perlene	EtOH	92
480-650	Fluorescein	NaOH 0.1M	84

By Eq.6, the fluorescence quantum yield is calculated as:

Compoound	Φ_{PL} (%) **4CzIPN**(m)	Φ_{PL} (%) **DAE-o/4CzIPN**(m)	Φ_{PL} (%) **DAE-c/4CzIPN**(m)
B-Carboline	15.61	3.85	0.34
Perlene	15.87	3.91	0.34
Fluorescein	14.13	3.48	0.31

14. Förster resonance energy transfer calculations

The efficiency of Förster resonance energy transfer *ET* was obtained by following equation:

$$ET = \frac{k_{ET}}{k_{ET} + \frac{1}{\tau_D}} = \frac{1}{1 + \left(\frac{R_{DA}}{R_0}\right)^6} \quad \text{Eq. 8}$$

The distance between the donor (**4CzIPN**) to acceptor (**DAE-c**) R_{DA} can be calculated by following equation[7]:

$$R_{DA} = \left((N_G) \times \frac{4\pi}{3}\right)^{-\frac{1}{3}} \quad \text{Eq. 9}$$

where N_G is the quantity of acceptor molecules in a unit volume. According to Samuel's report[8], the density of acceptor can be described as:

$$N_G = \beta \times \rho \times N_A / M_A \quad \text{Eq. 10}$$

where β is the fraction of acceptor in the micelle, ρ is the density of the micelle (assumed to be 1 g/cm^3), N_A is the Avogadro's constant and M_A is the molecular weight of the acceptor.

The Förster radius R_0 can be estimated by following equation:

$${R_0}^6 = \frac{9000(\ln 10)k^2\Phi_{PL}}{128\pi^5 N_A n^4} \int_0^\infty F_D(\lambda)\varepsilon_A(\lambda)\lambda^4 d\lambda \quad \text{Eq. 11}$$

where k^2 is orientation factor (k^2 is typically assumed to be 2/3 for the random orientation system), Φ_{PL} is the photoluminescence quantum yield of the donor in the absence of acceptor, N_A is Avogadro's constant, n is the refractive index of the medium, $J(\lambda) = \int_0^\infty F_D(\lambda)\varepsilon_A(\lambda)\lambda^4 d\lambda$ is the spectral overlap integral between PL of donor and absorption of acceptor, in which $F_D(\lambda)$ is the donor fluorescence normalized by area, $\varepsilon_A(\lambda)$ is the molar decadic extinction coefficient of acceptor and λ is the wavelength.

Table S4. Förster resonance energy transfer parameters of the micelle

Φ_{PL} (%)	$J(\lambda)$ (M^{-1} cm^{-1} (nm)^4)	R_0 (nm)	R_{DA} (nm)	ET (%)	k_{ET} (s^{-1})
4.1	4.21×10^{14}	1.96	1.22	94.50	6.86×10^{13}

15.The cellar Imaging of DS@M

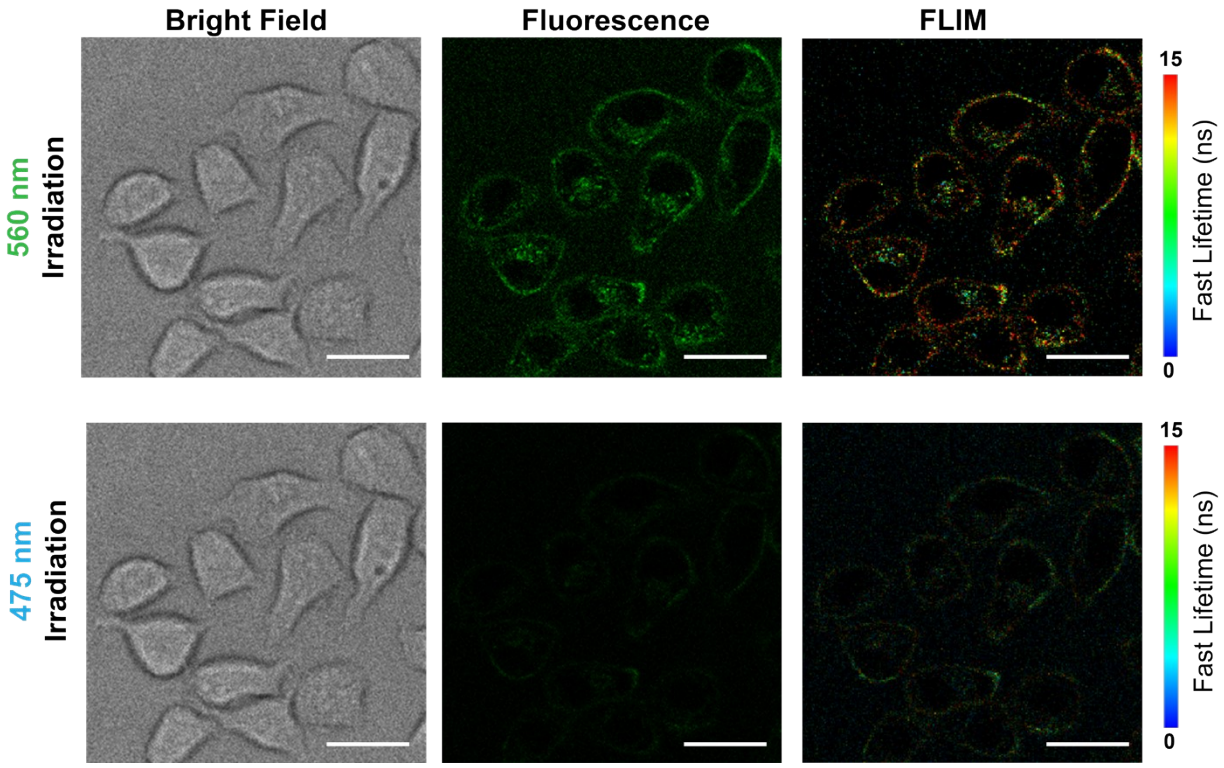

Figure S19. The bright field image, confocal fluorescent images and fluorescent lifetime images taken using a confocal laser scanning microscope (CLSM) after incubating HeLa cells with **DS@M** (10 μM), upon alternate irradiation with 475 nm/560 nm light (excitation: 475 nm; emission: 500−650 nm; irradiation with 475 nm: 10 mW/cm^2; irradiation with 560 nm: 30 mW/cm^2). Scale bar: 30 μm.

16. The colocalization of DS@M and Lyso-Tracker or Mito-Tracker

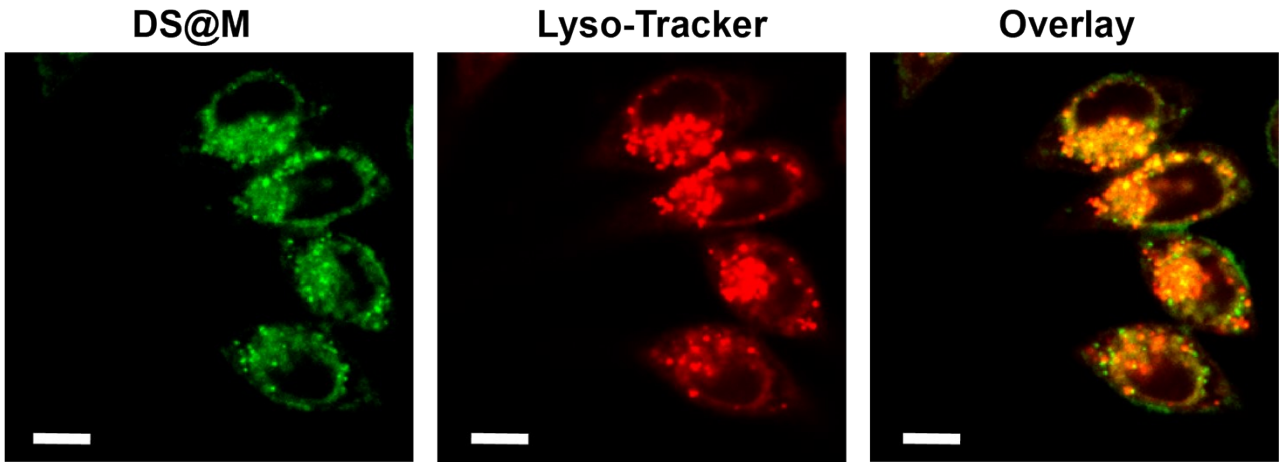

Figure S20. CLSM images of HeLa cells co-stained with **DS@M** (10 μM) and Lyso-Tracker Red (75 nM). Scale bar: 10 μm.

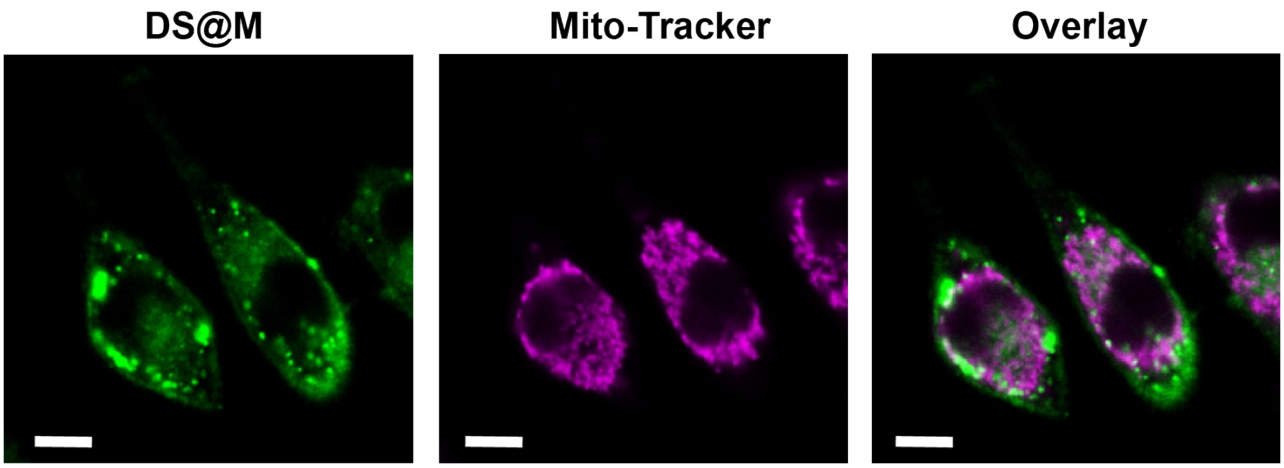

Figure S21. CLSM images of HeLa cells co-stained with **DS@M** and Mito-Tracker Deep Red. Scale bar: 10 μm.

17. In vitro cytotoxicity of DS@M

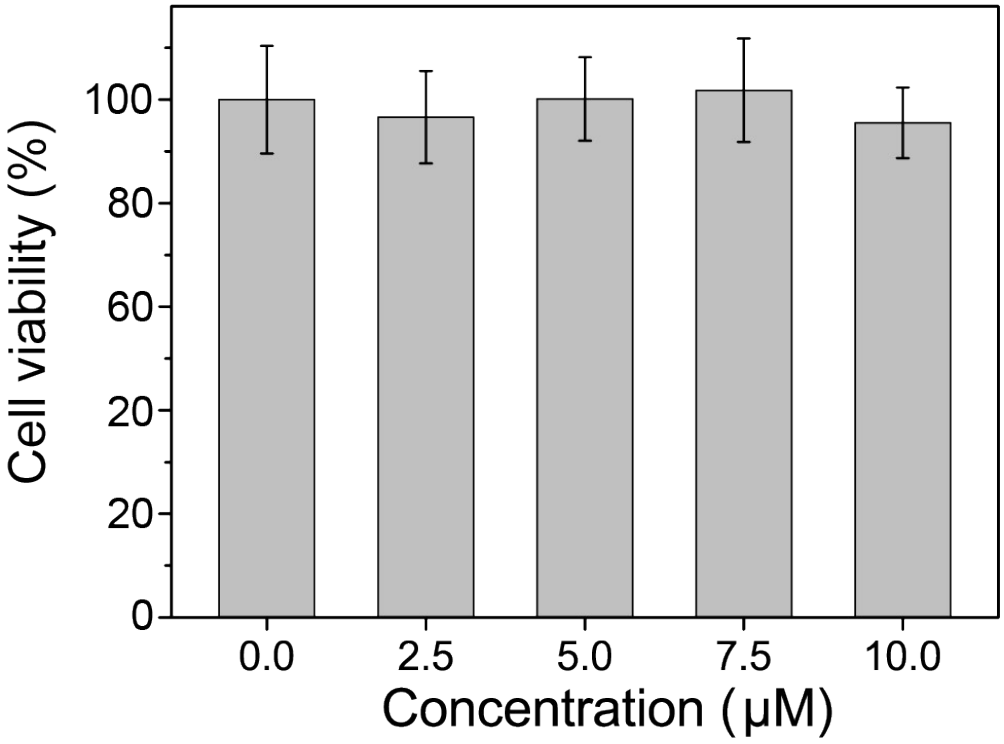

Figure S22. In vitro cytotoxicity of **DS@M** against HeLa cells at various concentrations for 12 h. The cell viability were evaluated by the CCK-8 assay.

18.Visible-Light Photo-Blinking of DS@M for Confocal Cellular Imaging

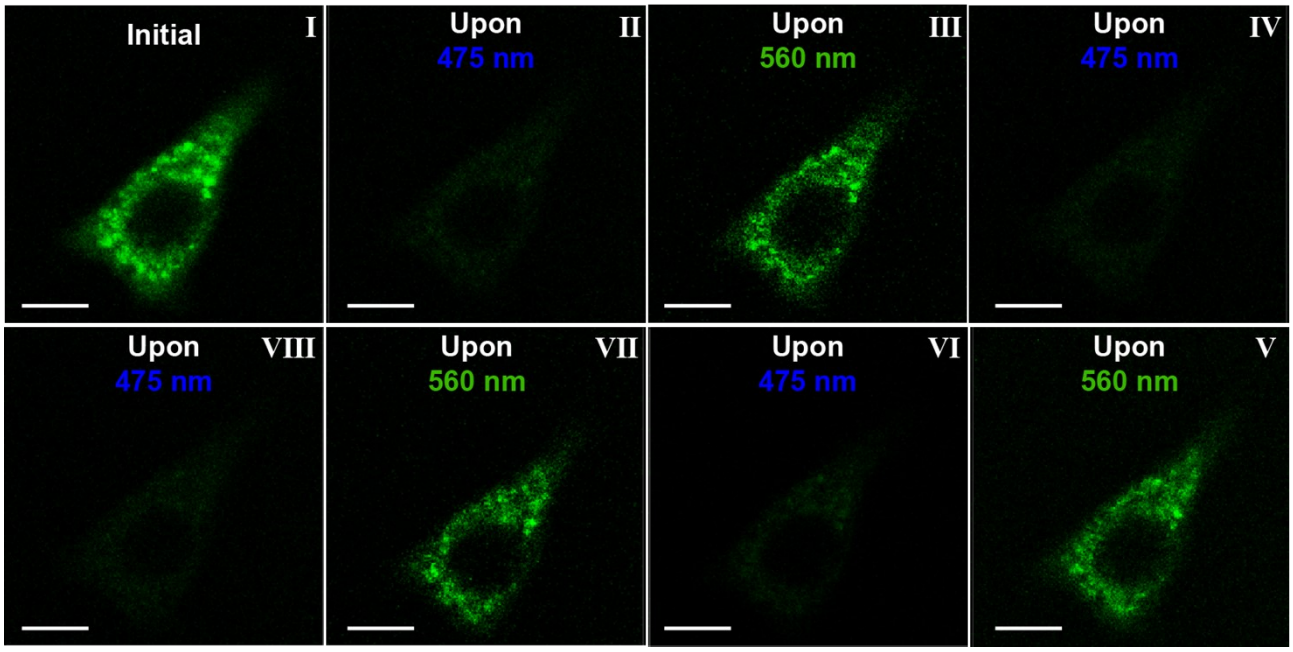

Figure S23. 475 nm and 560 nm irradiation cycling of fluorescence imaging of HeLa cells incubated with **DS@M** (10 μM) for 30 min, visualized by confocal laser-scanning microscopy (excitation: 475 nm; emission: 500-650 nm; scale bar = 10 μm).

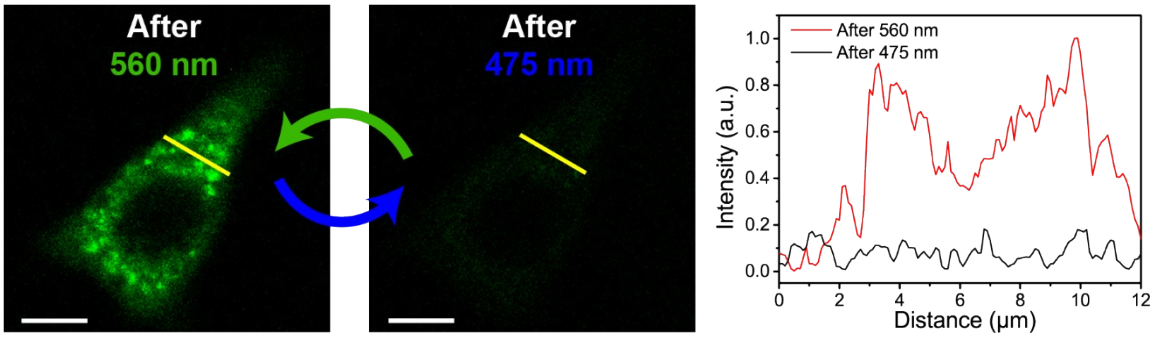

Figure S24. The fluorescence intensity of yellow line in HeLa cells upon 475/560 nm irradiation.

19. Visible-Light Photo-Blinking of DS@M for fluorescence lifetime imaging

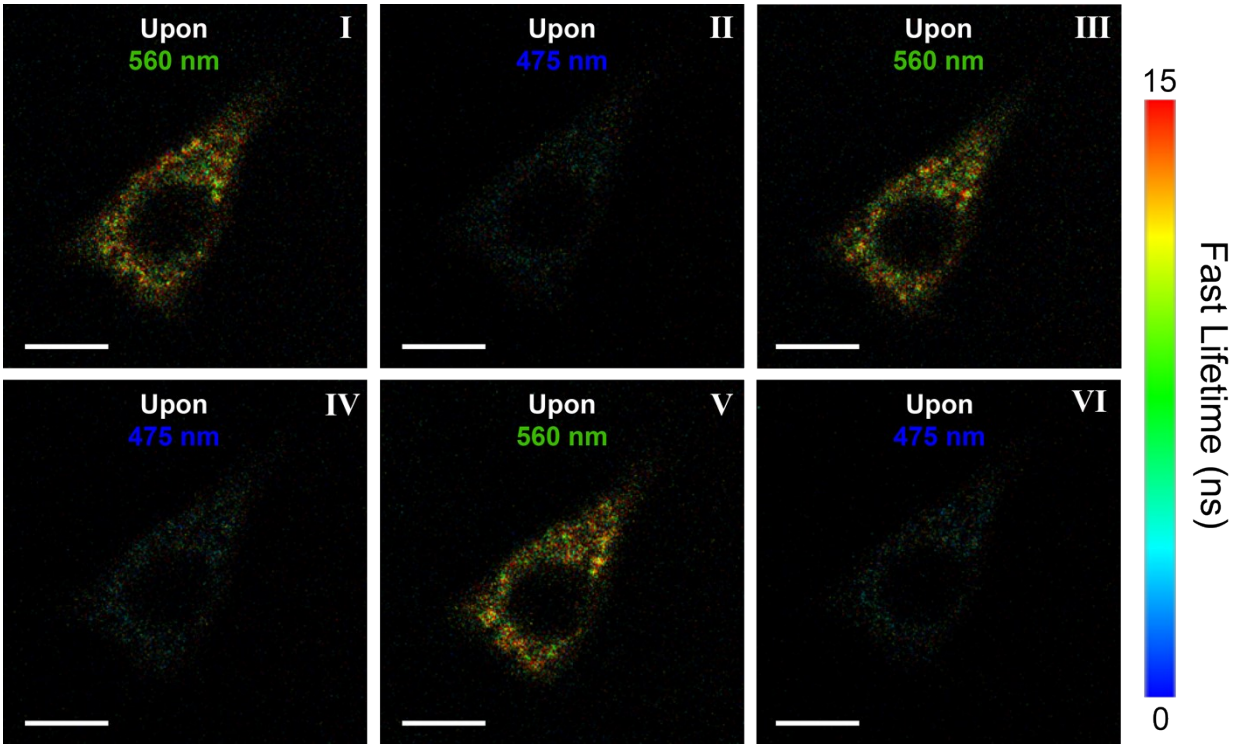

Figure S25. 475 nm and 560 nm irradiation cycling of fluorescence lifetime imaging of HeLa cells incubated with **DS@M** (10 μM) for 30 min, visualized by fluorescence lifetime imaging microscopy (excitation: 475 nm; emission: 500-650 nm; scale bar = 10 μm).

20. The Comparison of confocal and super-resolution images

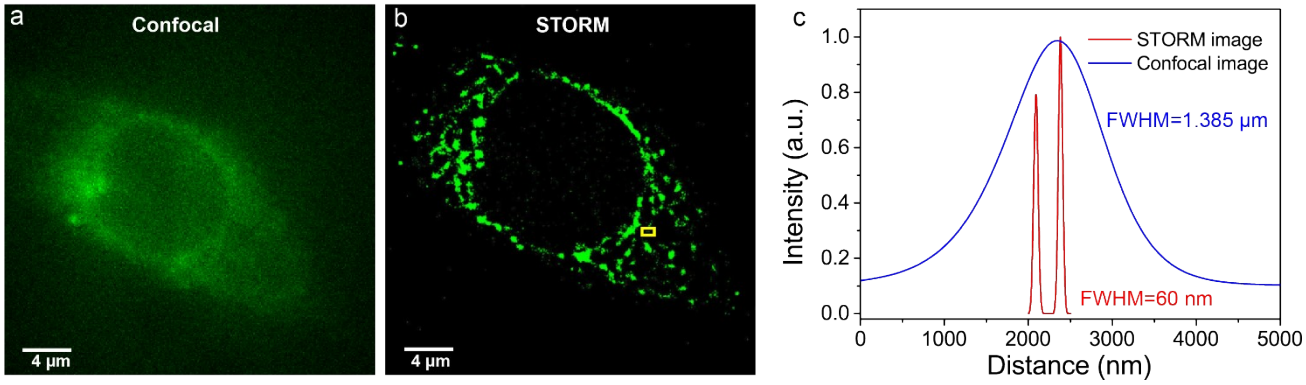

Figure S26. a) Confocal image of HeLa cells with **DS@M**; b) Super-resolution image (STORM) of HeLa cells with **DS@M**; c) The calculation of FWHM in HeLa cells of STORM image (red line, 60 nm) and confocal image (blue line, 1.385 μm).

21. The Fourier ring correlation (FRC) curve of super-resolution image

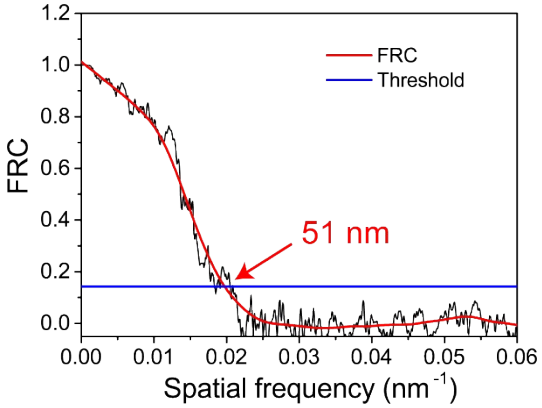

Figure S27. Fourier ring correlation (FRC) curve of the localizations presented in Figure 5c: FRC curve (black line), smoothed FRC curve (red line) and resolution threshold criterion 1/7 (blue line). The spatial resolution of the super-resolved image is calculated from the intersection between the FRC and the threshold, resulting in a value of about 51 nm.

22. References

[1]. S. Fredrich, R. Gostl, M. Herder, L. Grubert and S. Hecht, *Angew. Chem. Int. Ed.* 2016, **55**, 1208-1212.

[2]. T. Sumi, Y. Takagi, A. Yagi, M. Morimoto and M. Irie, *Chem. Commun*. 2014, **50**, 3928-3930.

[3]. W. J. Hehre, R. Ditchfield and J. A. Pople, *J. Chem. Phys.* 1972, **56**, 2257-2261.

[4]. T. Yanai, D. Tew and N. Handy, *Chem. Phys. Lett.* 2004, **393**, 51-57.

[5]. R. Krishnan, J. S. Binkley, R. Seeger and J. A. Pople, *J. Chem. Phys*. 1980, **72**, 650-654.

[6]. M. J. Frisch, et al. *Gaussian 09, revision D. 01*. (2009).

[7]. H. Wang, B. Yue, Z. Xie, B. Gao, Y. Xu, L. Liu, H. Sun and Y. Ma, *Phys Chem Chem Phys*, 2013, **15**: 3527-3534.

[8]. P. E. Shaw, A. Ruseckas, J. Peet, G. C. Bazan and D.W. Samuel, *Adv. Funct. Mater*. 2010, **20**, 155-161.